Polarization-dependent Mg($3p\ ^1P_1 \rightarrow 5s\ ^1S_0$, $4d\ ^1D_2$)–rare-gas-atom excited-state optical collisions: Experiment and theory

R. A. Lasell, B. S. Bayram, and M. D. Havey
Physics Department, Old Dominion University, Norfolk, Virginia 23529

D. V. Kupriyanov and S. V. Subbotin
Department of Theoretical Physics, St. Petersburg State Technical University, 195251 St. Petersburg, Russia
(Received 4 October 1996; revised manuscript received 24 March 1997)

Experimental spectra for excited-state optical collisions between Mg($3p\ ^1P_1$) atoms and rare-gas atoms are presented. Aligned Mg atoms are produced in the $3p\ ^1P_1$ level by excitation with linearly polarized light. Collisions between the excited metal atoms and Ne or Ar rare-gas atoms are probed in a 1000-cm^{-1} range in the vicinity of the Mg $3p\ ^1P_1 \rightarrow 5s\ ^1S_0$ and $3p\ ^1P_1 \rightarrow 4d\ ^1D_2$ transitions. The probe radiation is linearly polarized either along or perpendicular to the alignment axis, leading to a linear polarization for the optical collision process as a function of detuning of the probe from the atomic resonances. Substantial spectral variation of the linear polarization reflects the different molecular transitions responsible for the excitation process, and the evolution of the atomic alignment into the molecular regime. In the present case, the transitions correspond to excitation from the Mg–rare-gas $3p\ ^1\Pi_1$ and $3p\ ^1\Sigma_0^+$ molecular terms to the $5s\ ^1\Sigma_0^+$, $4d\ ^1\Delta_2$, $4d\ ^1\Pi_1$, and $4d\ ^1\Sigma_0^+$ terms. Experimental details of the approach, and the results obtained, will be described. Discussion of the polarization spectra is made through theoretical modeling focusing on the effects of the symmetry of the molecular states involved in the process. The modeling employs the semiclassical theory developed earlier. For a range of qualitatively correct interaction potentials and corresponding Condon points for the photo-excitation channels, good agreement between experiment and theoretical estimates is obtained. [S1050-2947(97)08108-0]

PACS number(s): 34.50.Rk, 34.80.Qb, 34.20.−b, 33.80.Gj

I. INTRODUCTION

Dissociative states of molecular complexes, ranging in size from large clusters to two-atom pairs, are important to a wide range of basic and applied collision phenomena [1–10]. In atomic collisions with energies typical of chemical forces, the intermediate dissociative states of a collision complex mediate exchange of energy, spin, charge, or fragments of the complex. However, experimental investigation and interpretation of the results are often made difficult by the transient nature of the states, and the normally very short lifetimes associated with them. Nevertheless, there is much motivation for study of such states, and many experimental approaches have been taken, for the transitional states and the nonadiabatic interactions between them are determinants of the details of collision or reaction dynamics.

Development of new techniques and technologies [4–7,9–15] for the study of transient states of small molecules has recently led to further elaboration of the amount of detail determinable directly from experiment. For example, collision experiments in atomic beams regularly select the initial internal atomic states, and determine the final ones as a function of scattering angles and energy [12]. These experiments can be complete in the sense that all measurable quantities associated with the full collision may be found by experiment. However, it is possible to determine additional information about the collision dynamics by probing the colliding pair during the collision process itself. This may be accomplished in the time domain by direct resolution of polarization or population dynamics on a femtosecond time scale [2], or in the frequency domain by nonresonant excitation of the colliding pair with moderately narrow-band light sources [3,4,10,11]. Recent elegant experiments [16] have demonstrated that it is possible to optically excite a colliding pair of atoms during a collision in the controlled environment of an atomic beam, and to selectively detect the excitation products. This approach promises to provide much more information concerning the collision than the traditionally complete atomic beam experiments.

Another technique [10,17] recently applied to studies of diatomic and triatomic collisions relies on the absorption of two photons during a single collision. This fractional collision process may be considered the frequency-domain analog of femtosecond-scale time domain studies, in that the excited-state molecular dynamics is both initiated and probed during the process. In the process, polarized light is absorbed by colliding pairs of atoms or molecules; this generally corresponds to generation of a superposition of molecular states. Absorption of polarized light of a different frequency from a second source reveals details of the rotational and vibrational dynamics. Mapping the frequency domain dynamics into a coordinate representation may be approximately accomplished through the classical Franck-Condon principle, which relates the frequency of the light absorbed to the difference potential surfaces relevant to the process [3].

In the present report, detailed experimental results and theoretical modeling are presented for collisional studies of atomic Mg($3p\ ^1P_1$) and the rare gases Ne or Ar. In the studies, a simplified variant of the fractional collision approach is employed. In it, absorption of linearly polarized light from a pump source takes place in the asymptotic regime, producing excited Mg atoms via the $3s\ ^1S_0 \rightarrow 3p\ ^1P_1$

resonance transition. This generates an electronic alignment in the $3p\ ^1P_1$ level. Collisions with the rare-gas atoms transport the alignment into the molecular regime, where it is probed by a second linearly polarized light source. Varying the relative polarization directions of the two light sources generates a linear polarization spectrum as a function of the frequency of the second light source. The polarization spectrum for this process, termed an excited-state optical collision, depends on both the detailed evolution of the alignment during the collision and the symmetry of the molecular terms accessed in the probe phase. In the present work, the alignment is probed in the vicinity of the atomic Mg $3p\ ^1P_1 \rightarrow 5s\ ^1S_0$ and $3p\ ^1P_1 \rightarrow 4d\ ^1D_2$ transitions, thus accessing $5s\ ^1\Sigma_0^+$, $4d\ ^1\Delta_2$, $4d\ ^1\Pi_1$, and $4d\ ^1\Sigma_0^+$ molecular terms. Focus in the present work is primarily on the $4d$ channels and on the possibility of inelastic processes leading to the $5s\ ^1S_0$ singlet or $5s\ ^3S_1$ triplet channels; we have reported previously on direct excitation in the vicinity of the $5s\ ^1S_0$ level [11]. Theoretical modeling of the process can reveal both the alignment dynamics and the weights of the various molecular transitions contributing to the process.

In the present paper, the details of the experimental approach will first be described, including the excitation and detection scheme for the process. This will be followed by presentation of the results and discussion of systematic effects on the measurements. The theoretical sections will first be concerned with the general properties of the interatomic potentials. This will be followed by discussion of the experimental results through a semiclassical model of the process developed earlier for optical collisions of polarized atoms [18], using plausible, qualitatively correct interatomic potentials. The main tool employed for the discussion will be *estimates* of the range of linear polarization values possible for allowed optical transitions between each pair of molecular terms, and ignoring interference.

II. EXPERIMENTAL APPROACH

The basic physical scheme of the experiment is similar to that employed in our earlier work [11], and so will be only briefly described here. The approach is illustrated in Fig. 1, which shows the relevant atomic Mg energy levels and qualitative Mg–rare-gas interatomic potentials. In the scheme, aligned and excited Mg atoms are produced in the $3p\ ^1P_1$ level by resonant excitation at 285.2 nm with laser 1, which is linearly polarized along a z axis. In the absence of collisions, only atomic stepwise excitation is possible on the Mg $3p\ ^1P_1 \rightarrow 5s\ ^1S_0$ and $3p\ ^1P_1 \rightarrow 4d\ ^1D_2$ transitions at 571.2 and 552.8 nm. This is accomplished with a second, linearly polarized probe laser 2. Signals in each case may be monitored at 202.6 nm on the $4p\ ^1P_1 \rightarrow 3s\ ^1S_0$ cascade transition. The alignment in the $3p$ level is probed by measuring the signal I_{zz} when laser 1 and laser 2 are linearly polarized along the same line, and I_{zx} when they have orthogonal linear polarizations. The alignment is determined through the experimentally convenient linear polarization ratio

$$P_L = \frac{I_{zz} - I_{zx}}{I_{zz} + I_{zx}}. \tag{1}$$

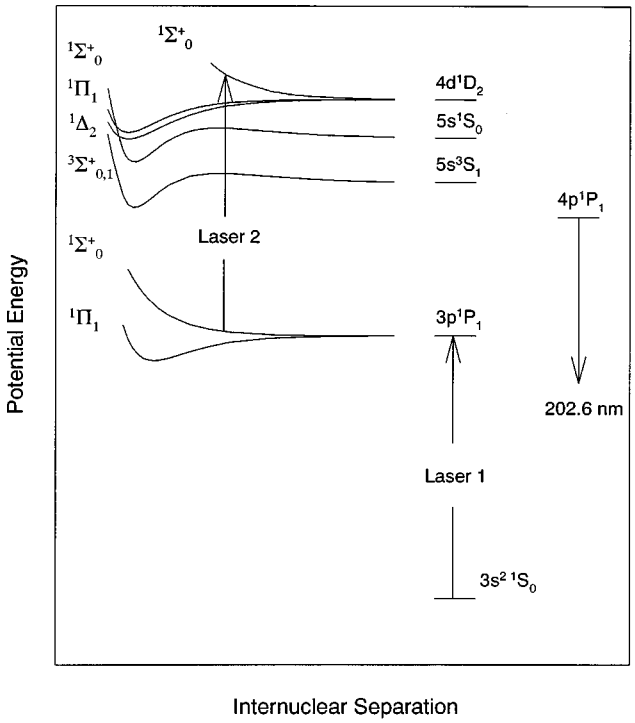

FIG. 1. Qualitative interaction potentials for several magnesium–rare-gas electronic states, and an illustration of the experimental scheme.

In the absence of hyperfine, Zeeman, or collisional depolarization in the $3p\ ^1P_1$ level, the linear polarization values expected on these transitions are $P_L = 1$ (100%) ($3p\ ^1P_1 \rightarrow 5s\ ^1S_0$ transition) and $P_L = 1/7$ (14.3%) ($3p\ ^1P_1 \rightarrow 4d\ ^1D_2$ transition).

When collisions are considered, excitation by laser 2 can occur even when the atomic resonance condition is not met. These excited-state optical collisions occur because of optical electronic transitions in the transient Mg–rare-gas molecules formed during binary Mg atom and rare-gas atom collisions. As illustrated in Fig. 1, the transitions occur in the vicinity of stationary phase points localized at internuclear separations R, which may be estimated by application of the classical Frank-Condon principle. Defining a detuning $\Delta = hf_2 - hf_{20}$, where hf_{20} is the atomic Mg $3p\ ^1P_1 \rightarrow 4d\ ^1D_2$ transition energy, transitions occur for internuclear separations R satisfying $U_U(R) - U_L(R) = \Delta$, where $U_U(R)$ and $U_L(R)$ are upper and lower term potentials. Inspection Fig. 1 shows that in the present case there are numerous potentials in the same energy range, leading to the likelihood that several roots R will contribute to optical excitation at a specified detuning.

Because the precursor excited Mg atoms are aligned, the transient molecules formed in collision will be also, although the amount of molecular alignment will depend on recoupling of the atomic angular momentum into the molecular frame and on the integrated effects of molecular rotation, during the course of the collision, in the Mg–rare-gas $3p\ ^1\Pi_1$ and $3p\ ^1\Sigma_0^+$ electronic states. Following molecular excitation, the Mg–rare-gas molecules dissociate, producing Mg atoms in the $5s\ ^1S_0$ and $4d\ ^1D_2$ levels. In a previous report we described the results of experiments with detunings such that primarily the $5s\ ^1\Sigma_n^+$ state was produced.

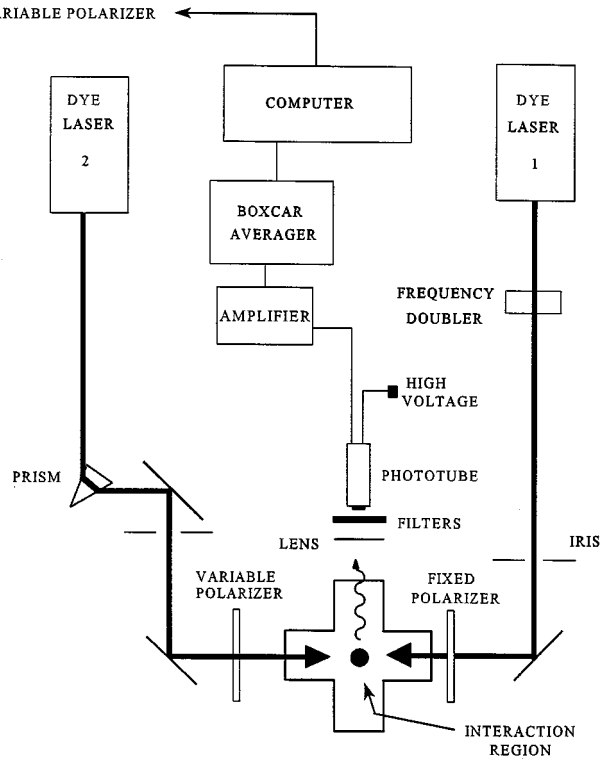

FIG. 2. A block diagram of the experimental apparatus.

Present measurements are concerned with excitation in the vicinity of the $4d\ ^1D_2$ level, for which the $4d\ ^1\Lambda_\Omega$ terms dominate. However, some excitation of the $5s\ ^1\Sigma_0^+$ state is possible, either by direct optical excitation or by nonadiabatic Coriolis coupling with the optically excited $4d\ ^1\Pi_1$, state. This is monitored by a second detection channel that observes the $5s\ ^1S_0 \rightarrow 3p\ ^1P_1$ fluorescence at 571.2 nm. Finally, there remains the possibility of spin-orbit-coupling–induced nonadiabatic transitions to the $5s\ ^3\Sigma_1^+$ state. Thus, the second detection channel can be replaced as needed so that the $5s\ ^3S_1 \rightarrow 3p\ ^3P_j$ triplet series fluorescence around 333 nm can instead be monitored.

A schematic diagram of the experimental apparatus is shown in Fig. 2. There, two pulsed dye lasers are pumped by the second harmonic of a neodymium:yttrium aluminum garnet (Nd:YAG) laser at 532 nm. The grazing incidence dye lasers produce 100-μJ, 6-ns pulses having an approximately 3-GHz bandwidth. The laser outputs are strongly linearly polarized in a horizontal plane. The output of each laser is passed through separate amplifiers, increasing the pulse energy by about a factor of 10. Laser 1 is then focused into a potassium dihydrogen phosphate doubling crystal. A glass absorption filter is then used to remove the residual fundamental, but permitting about 85% of the desired 285.2-nm radiation. The frequency-doubled output typically has 30-μJ pulses, which were attenuated to less than 1 μJ in order to avoid saturation of the Mg resonance line. Laser 2, which operates near 552.8 nm, has its output spectrally filtered to remove broadband fluorescence from the beam. This is essential in the experiments, for the relatively low level fluorescence is sufficient to produce signals larger than the desired ones due to the excited-state optical collision process. When laser 2 is tuned to stepwise atomic resonance, its power is attenuated by about 10^4, in order to avoid saturation of the atomic transition.

The laser 2 beam passes through a liquid-crystal variable waveplate, the retardance of which may be varied by changing the voltage applied to the device. The optic axis of the liquid crystal is set at 45° from the laser's initial linear polarization direction. Thus with zero retardance, the polarization is unchanged from its horizontal orientation but with the crystal voltage set for half-wave retardance, the polarization is rotated by 90°. The device produces linearly polarized light with a polarization purity of better than 10^{-3}. This is assessed by both contrast ratio tests and by a 45° test. In the contrast ratio test, the transmission of the laser radiation through the liquid-crystal retarder and through an orthogonal Glan-Thompson polarization analyzer is measured. In a 45° test, the Glan-Thompson analyzer is oriented at 45° to the initial polarization direction. Then an *in situ* polarization measurement [viz. Eq. (1)] should measure zero for P_L. This demanding test typically yields $P_L < 0.002(2)$, limited by counting statistics.

The two laser beams are collinear, but propagate in opposite directions through the sample cell. The beams each have a diameter of about 0.5 cm in the interaction region of the cell. The sample cell consists of a 250-ml Pyrex bulb mounted with two sidearms, located on opposite sides of the cell and at right angles to the laser beams, for fluorescence viewing. Two other sidearms allow for passage of the laser beams. As described elsewhere [10,17], an internally heated boat containing Mg chips generates a metal atom density of about 10^{11} cm^{-3} in the central region of the cell. Connection of the cell to a vacuum-gas handling system allows for evacuation to less than 10^{-7} Torr, and for admission of research grade rare gases. The rare-gas pressure is determined by a capacitance manometer, which is calibrated against an oil manometer. Because of the method of vaporizing the Mg, the metal vapor and the rare gas are at an estimated temperature of 330 K. One detection channel monitors the $4p\ ^1P_1 \rightarrow 3s\ ^1S_0$ cascade transition at 202.6 nm. This channel is sensitive to population in both the $5s\ ^1S_0$ and $4d\ ^1D_2$ levels, although the branching ratios strongly favor the $4d\ ^1D_2$ level [19]. A photomultiplier tube (bialkali cathode) mounted with two narrow-band interference filters pass only about 2% of the desired radiation, but eliminate the very intense resonance radiation and other background light such that it is at most 10% of the weakest molecular signals. The second detection channel is normally used to monitor the $5s\ ^1S_0 \rightarrow 3p\ ^1P_1$ fluorescence at 571.2 nm, thus providing a relative measure of the $5s\ ^1S_0$ population. The photomultiplier (PMT) used to obtain the signals has a bialkali cathode, and is mounted with three narrow-band interference filters and two colored-glass cutoff filters to eliminate residual green light from entering the cell (primarily background from the YAG pump laser). The signal-to-noise ratio is strong enough for excitation in the vicinity of the $4d\ ^1D_2$ level, but reliable measurements could be obtained only for detunings $\Delta < 25$ cm^{-1}. As indicated earlier, auxiliary measurements were also made in this second channel in order to measure possible intersystem transfer to the $5s\ ^3S_1$ level. A

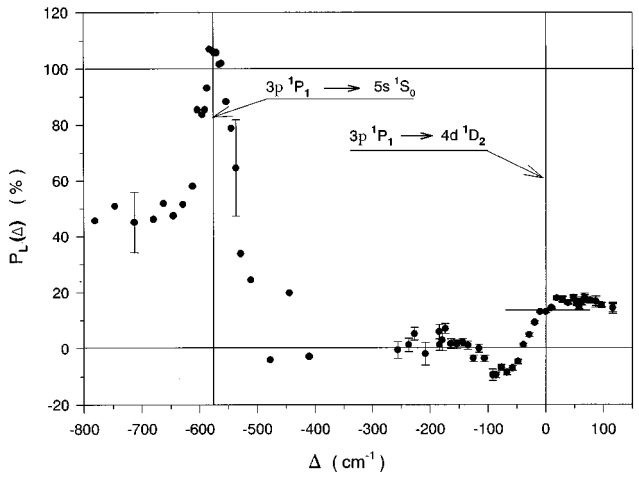

FIG. 3. Polarization spectrum for Mg-Ne excited-state optical collisions. The spectrum is presented for the zero-pressure limit. The origin of detuning ($\Delta=0$) corresponds to the atomic Mg $3p\ ^1P_1 \rightarrow 4d\ ^1D_2$ transition.

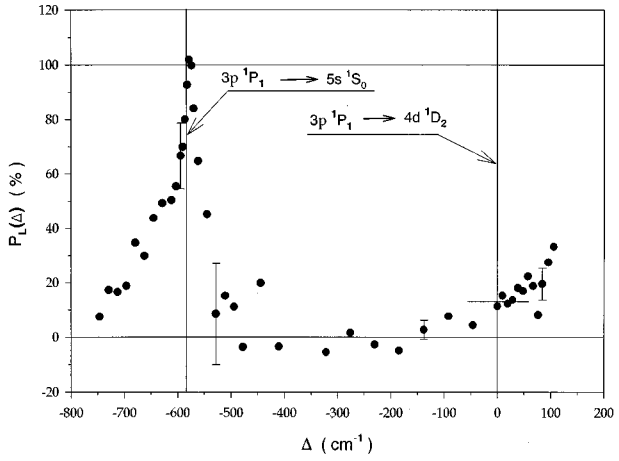

FIG. 4. Polarization spectrum for Mg-Ar excited-state optical collisions. The spectrum is presented for the zero-pressure limit. The origin of detuning ($\Delta=0$) corresponds to the atomic Mg $3p\ ^1P_1 \rightarrow 4d\ ^1D_2$ transition.

narrow-band interference filter centered at 330 nm and two ultraviolet transmitting glass filters were used to select the $5s\ ^3S_1 \rightarrow 3p\ ^3P_j$ transitions.

The output from each PMT was amplified, integrated over a 200-ns gate in a boxcar averager. The resulting signals were digitized and stored in a laboratory computer for later analysis. The data were collected in runs consisting of 2000 laser shots, partitioned into two halves. In each half there was a datum and a background run for each polarization direction, with the order of data taking in each polarization channel reversed for the two halves. This minimized the effects of laser power and frequency drift on the polarization measurements.

III. EXPERIMENTAL RESULTS AND GENERAL DISCUSSION

The measured linear polarization spectra $P_L(\Delta)$, as determined by monitoring the main $4p\ ^1P_1 \rightarrow 3s\ ^1S_0$ signal channel, for Mg-Ne and Mg-Ar excited-state optical collisions are presented in Figs. 3 and 4. In each case, the data for detunings $|\Delta| > 450\ \text{cm}^{-1}$ are reproduced from Lasell, *et al.* [11] in order to facilitate comparison with new data taken at smaller detunings and to make comparisons with the theoretical calculations described in a later section.

In the data, the uncertainty in the horizontal detuning scale of $\pm 1\ \text{cm}^{-1}$ is negligible on the scale of the figures. The indicated vertical error bars on the polarization $P_L(\Delta)$ are from a combination of statistical errors in the measurements and from an extrapolation of the data to a single collision limit. The origin of the pressure dependence is collisional disalignment of the Mg $3p\ ^1P_1$ atoms prior to excitation during a collision with laser 2. To illustrate the effect, characteristic pressure-dependent data for Mg-Ne are presented in Fig. 5. As described in earlier work, the nearly linear curves represent fits to the data accounting for the collisional depolarization, radiative decay, and the finite pulsewidth of the pump and probe lasers. These fits yield a collisional depolarization rate coefficient for the disalignment collisions; the results of modeling the laser pulses as temporally constant or triangular, and with a width $T = 6.0$ ns, are presented in Table I. As in our earlier work, the uncertainty in the rate coefficient k is larger than the differences between the two models. Thus we simply average the results. The average is seen to be consistent, within the combined error bars, of the values for k reported earlier. The measured average rate coefficients are used to extrapolate data taken at $P = 20$ Torr to a single collision limit, as presented in the figures. Other than the pressure dependence, the measured polarization spectra are free of measurable systematic effects due to laser power, Mg density, or systematic variations in background light. Signals due to amplified

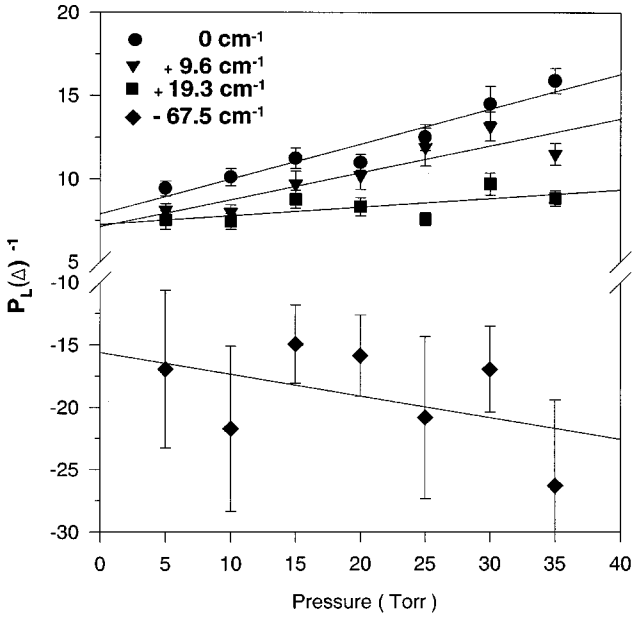

FIG. 5. Illustrative pressure dependence at selected detunings for Mg-Ne excited-state optical collisions. The zero-pressure intercept of each line gives the zero-pressure limit, represented as the data points in Figs. 3 and 4.

TABLE I. Rate coefficients at $T=330$ K for depolarization of the atomic Mg $3p\ ^1P_1$ level by collisions with the rare gases Ne and Ar.

k (10^{-10} cm^3/s)		
Mg-Ar	Mg-Ne	Reference
9.4(5)	6.5(7)	Lasell *et al.* [11]
9.6(5)	6.7(7)	This work

spontaneous emission from the two lasers were negligible compared to the optical collision signals.

Generally, the measured polarization is seen to undergo strong variations with detuning. But, as expected, in the limit of no depolarizing collisions, the measured polarization is $P_L(\Delta=-578.3\ \text{cm}^{-1})=100(2)\%$ at the atomic Mg $3p\ ^1P_1 \rightarrow 5s\ ^1S_0$ transition, and $P_L(\Delta=0\ \text{cm}^{-1})=14(1)\%$ at the atomic $3p\ ^1P_1 \rightarrow 4d\ ^1D_2$ transition. The agreement of these values with those expected for these atomic transitions is a measure of the quality of the polarimeter used to make the linear polarization measurements. Qualitatively, the variations of polarization with detuning are similar for Mg-Ne and Mg-Ar excited-state optical collisions. Particularly notable for the new data in the vicinity of the $3p\ ^1P_1 \rightarrow 4d\ ^1D_2$ transition is the quite rapid variation from a value *larger* than the atomic value when $\Delta>0$ to a *negative* range when $\Delta<0$. To our knowledge, this represents the first time that collision-induced absorption in an optical collision has yielded a larger value for the polarization than that for the associated resonance transition. As will be discussed later in this report, the variations of polarization with detuning are due to the type of molecular transitions responsible for absorption at a specific detuning, the recoupling of the atomic alignment into the molecular frame, and the rotation of the molecular axis during the collision.

As discussed above, an experimental effort was made to directly observe inelastic scattering into the $5s\ ^1S_0$ and $5s\ ^3S_1$ levels. For the singlet channel, direct excitation of the $4d\ ^1D_2$ level generated a weak signal originating in the $5s\ ^1S_0$ level, indicating that there are some nonadiabatic interactions between the molecular terms associated with these levels. For detunings within about 25 cm^{-1} of direct excitation, it was possible to detect signal in the inelastic singlet channel. However, the ratio of intensity in this channel compared to the main channel did not vary with detuning. Further, comparison of the ratio of the intensities in the inelastic to main channel revealed a linear pressure dependence with zero intercept. Thus, the observed signals in the inelastic singlet channel are apparently due to subsequent collisions of rare-gas atoms with the Mg($4d\ ^1D_2$) atoms; the spectral region associated with the inelastic process was not directly accessed in these experiments. Inelastic collisions mediated by the spin-orbit interaction can produce intersystem population transfer. As discussed, we searched for this possibility by setting up one detection channel sensitive to population generated in the $5s\ ^3S_1$ level, which is 680 cm^{-1} lower in energy than the $5s\ ^1S_0$ level. However, no signal was detected in this channel, even for resonant excitation of the atomic singlet levels. Apparently the much weaker spin-orbit interaction in Mg, in comparison to Ca (where intersystem collisional crossing has been observed), is insufficient to generate measurable population in this channel, in comparison to the main singlet one.

IV. THEORY: Mg–RARE-GAS INTERACTION POTENTIALS

The theoretical sections are organized into two parts. In the first part, *qualitative* discussion is made of the interatomic interaction of highly excited magnesium and rare-gas atoms. General peculiarities of the behavior of excited molecular potentials, which are important for the following semiclassical calculations of optical collision cross sections, are ascertained. In the second portion, we make numerical estimates of the polarization signal for the different spectral domains examined in experiment. The estimates are based on a semiclassical approach developed earlier for polarized-atom optical collisions [18], i.e., on a quantum description of the electronic subsystem combined with a classical description of the motion of atomic nuclei. However, in the absence of quantitatively reliable interatomic potentials for the important molecular terms in Mg-Ne and Mg-Ar, the detuning-dependent linear polarization is not calculated. Instead, plausible estimates of the interatomic potentials are used to find ranges of Condon points for the allowed transitions, and to describe the collision dynamics in the lower terms. A partial polarization is determined for the transition at each Condon point. These results are then used to establish upper and lower bounds on the polarization. These bounds, and the qualitative shapes of the interatomic potentials, then form the basis of the discussion of the experimental results.

A. Magnesium–rare-gas-atom potentials correlated with Mg($5s\ ^1S_0$, $5s\ ^3S_1$, $4d\ ^1D_2$)

The interaction of alkaline-earth atoms with rare-gas atoms has been considered theoretically by several groups [20–23]. The calculation of the potentials for the Mg-Ne system were done by Malvern [20] and Czuchaj *et al.* [21] and for Mg-Ar by Hliwa and Daudey [22]. The numerical results of these authors cover the energy domain from the ground state, with $3s^2$ electronic configuration, to all possible excited states of the magnesium atom up to the $3s3p$ and $3s4p$ configurations. The precise evaluation of molecular potentials in the energy domain near the $3s5s\ ^1S_0$, $3s5s\ ^3S_1$, and $3s4d\ ^1D_2$ states has some specific difficulties because of the many atomic configurations that should be included in numerical calculations. However, to make clear the following analysis of polarization-dependent Mg–rare-gas-atom optical collisions, we briefly discuss a qualitative picture of the interatomic interactions.

The interaction of a highly excited alkaline-earth atom with a rare-gas atom can be considered in a pseudopotential approximation [24,25]. In such an approximation the highly excited orbital can be described as a single electronic state in an effective potential. This potential is determined by the self-consistent field (SCH) of the core electrons and can include long-range polarization interactions with the molecular core. The N-electron wave function with one highly excited electron in the outer shell for a diatomic system at internuclear separation R can be expressed as follows:

$$\Psi_{\lambda\tilde{\Lambda}\sigma\tilde{\Sigma}}(\mathbf{r}_1\xi_1,\ldots,\mathbf{r}_N\xi_N;R)$$
$$=\frac{1}{\sqrt{N}}\sum_p(-1)^p\hat{P}\,\phi'_{n\lambda\sigma}(r_1\xi_1;R)$$
$$\times\widetilde{\Psi}_{\tilde{\Lambda}\tilde{\Sigma}}(r_2\xi_2,\ldots,r_N\xi_N;R). \quad (2)$$

Here λ and σ are the electronic and spin angular momentum projection of the excited electron and n describes other quantum numbers of the orbital. The $\widetilde{\Psi}_{\tilde{\Lambda}\tilde{\Sigma}}$ is the wave function of the Mg–rare-gas molecular ion core and $\tilde{\Lambda},\tilde{\Sigma}$ are the orbital and spin angular momentum projections, respectively. The sum in Eq. (2) is over all possible transpositions p of the space position and spin coordinates $\mathbf{r}_1,\xi_1$ of the excited orbital and corresponding coordinates of core electrons $\mathbf{r}_i,\xi_i$ with $i=2,\ldots,N$, which are generated by transposition operators. The orbital and spin core quantum numbers are $\tilde{\Lambda}=0$, $\tilde{\Sigma}=\pm\frac{1}{2}$ and for the total orbital Λ and spin Σ angular momenta projections we obtain $\Lambda=\lambda$, $\Sigma=\tilde{\Sigma}+\sigma$.

The excited electron wave function $\phi'_{n\lambda\sigma}(\mathbf{r}\xi;R)$ can be introduced as the projection of a so-called pseudo-orbital wave function $\phi_{n\lambda\sigma}(\mathbf{r}\xi;R)$ on a space orthogonal to the core orbitals

$$\phi'_{n\lambda\sigma}=(1-\hat{T}_c)\,\phi_{n\lambda\sigma}, \quad (3)$$

where $\hat{T}_c$ is the core projection operator [24]. In a nonrelativistic approximation the pseudo-orbital can be expressed as $\phi_{n\lambda\sigma}(\mathbf{r}\xi;R)=\phi_{n\lambda}(\mathbf{r};R)\chi_\sigma(\xi)$, where $\chi_\sigma(\xi)$ is the spin function, and the space-coordinate-dependent wave function $\phi_{n\lambda}(\mathbf{r};R)$ satisfies the following Schrödinger equation (in a.u.):

$$[-\tfrac{1}{2}\Delta+\hat{V}_{\rm eff}(\mathbf{r},R)]\,\phi_{n\lambda}(\mathbf{r};R)=U^{(1)}_{n\lambda}(R)\,\phi_{n\lambda}(\mathbf{r};R), \quad (4)$$

where $\hat{V}_{\rm eff}(r,R)$ is the effective interaction operator for the $n\lambda$ shell and $U^{(1)}_{n\lambda}(R)$ is the corresponding energy of the electron. In a self-consistent field approximation the total interaction energy of the system described by the wave function (2) is

$$U_{n\Lambda}(R)=U^{(1)}_{n\lambda}(R)+U(R), \quad (5)$$

where the second term is the core interaction, which can be expressed as the average of Hamiltonian $\hat{H}^{(N-1)}$ for the $N-1$ electron system over the wave function $\widetilde{\Psi}_{\tilde{\Lambda}\tilde{\Sigma}}$:

$$U(R)=\langle\widetilde{\Psi}_{\tilde{\Lambda}\tilde{\Sigma}}|\hat{H}^{(N-1)}|\widetilde{\Psi}_{\tilde{\Lambda}\tilde{\Sigma}}\rangle. \quad (6)$$

This core contribution to the interatomic interaction does not depend on spin projection $\tilde{\Sigma}\pm\frac{1}{2}$ or on $\tilde{\Lambda}=0$ in our case. It is assumed here that the potential $U(R)$ reproduces only the short-range part of the core interaction in the SCF approximation; i.e., the atomic orbital approximation of internal molecular orbitals, with the following determinant reduction of the wave function $\widetilde{\Psi}_{\tilde{\Lambda}\tilde{\Sigma}}$, is used.

It is convenient and more correct to include long-range polarization (asymptotically $\sim R^{-4}$) of the core directly in the effective potential (5) because, at large R, the interference should be between both types of rare-gas-atom polarizations, that is, polarization both by the metal ion and the excited electron. In the SCF approximation, the adiabatic potential depends only on configuration quantum numbers n and on total angular momentum projection Λ (or λ) as is shown by Eq. (5). In this step only exchange interaction in closed shells of the molecular core is to be taken into account. However, the exchange interaction between the excited orbital and the upper $\sigma 3s$ orbital of the molecular core, which is mainly a $Mg^+(3s)$ atomic orbital, leads to the splitting between the states with different values of total spin quantum number S. To estimate this splitting we introduce, instead of wave function (2), wave functions with a definite value of S: $\Psi_{\Lambda S\Sigma}(\ )$. We omit here and below the symbolic quantum number $\tilde{\Lambda}=0$ and use Λ instead of λ as a wave function quantum index. The singlet-state $S=0$ wave function is

$$\Psi_{\Lambda 00}(\ )=\frac{1}{\sqrt{2}}[\Psi_{\Lambda\,1/2-1/2}(\ )-\Psi_{\Lambda-1/21/2}(\ )] \quad (7)$$

and the triplet-state $S=1$, $\Sigma=\pm1,0$ wave functions are

$$\Psi_{\Lambda 1\pm1}(\ )=\Psi_{\Lambda\pm1/2\pm1/2}(\ ), \quad (8)$$

$$\Psi_{\Lambda 10}(\ )=\frac{1}{\sqrt{2}}[\Psi_{\Lambda\,1/2-1/2}(\ )+\Psi_{\Lambda-1/21/2}(\ )].$$

The exchange potential splitting caused by the excited orbital and core exchange interaction can be estimated by averaging of the total Hamiltonian $\hat{H}^{(N)}$ for the N-electron system over these wave functions. We expect that in accordance with Hund's rule the triplet state described by wave function (8) has less energy because of a less repulsive interaction between the excited and $\sigma 3s$ orbitals.

To estimate the excited orbital energy $U^{(1)}_{n\lambda}(R)$ we consider the $\hat{V}_{\rm eff}$ interaction as the sum

$$\hat{V}_{\rm eff}=\hat{V}^{(1)}_{\rm eff}+\hat{V}^{(2)}_{\rm eff}, \quad (9)$$

where $\hat{V}^{(1)}_{\rm eff}$ is the interaction with the core and the $3s$ orbital of magnesium atom and $\hat{V}^{(2)}_{\rm eff}$ is the interaction with the rare-gas atom. The first interaction is described mainly by the SCF of the metal atom electrons and includes the short-range repulsive interaction and the long-range Coulomb attraction. We ignore here the polarization effects for the $3s$ shell and core electrons of the magnesium atom. The second interaction can be represented as the sum of a short-range rare-gas atom effective potential $\hat{V}^{(s)}$ and a polarization contribution of the valence shell of this atom induced both by interactions with the magnesium ion and with the excited electron. It can be presented in the following form [25]:

$$\hat{V}^{(2)}_{\rm eff}=\hat{V}^{s}-\frac{\alpha_2}{2}\left(\frac{1}{R^4}+\frac{1}{r^4}+\frac{2\cos\theta}{r^2R^2}\right), \quad (10)$$

where α_2 is the dipole polarizability of the rare-gas atom. The r coordinate, as well as the polar angle θ, relate to the rare-gas-atom coordinate frame.

With the assumptions described above we can recover the following qualitative picture of the potential's behavior. For an internuclear separation R that is larger than the average radial location for the excited electron, the electron energy $U^{(1)}_{n\lambda}(R)$ and the potential (5) reduce to a dispersive interaction between rare-gas and metal atoms, $U^{(1)}_{n\lambda}(R) \propto R^{-6}$. This asymptotic interaction can be obtained if we treat the pseudo-orbital as an excited atomic orbital of the metal atom in the $\hat{V}^{(1)}_{\rm eff}$ potential and expand the second term in Eq. (10) assuming an electron localized near the metal atom core. All the adiabatic potentials should be negative relative to the corresponding asymptotic atomic energy levels in this region of internuclear separation. In the asymptotic region, potentials correlating with the $3s4d\ ^1D_2$ level and a ground-level rare-gas atom have the following energy ordering: the $^1\Sigma^+_0$ potential should be lower in energy than that for the $^1\Pi_1$ term, while the $^1\Pi_1$ potential should be lower than that of the $^1\Delta_2$ term. As indicated in Fig. 1, this ordering is reversed at shorter range.

To estimate the energy $U^{(1)}_{n\lambda}(R)$ at an internuclear separation comparable with the characteristic orbital radius of the excited electron, the multiple scattering method can be applied [25,26]. This method is based on the idea of analytical continuation of the Schrödinger equation (4) in integral form (which is normally used in scattering problems) from small positive to small negative energy values. It gives an analytical result for the σ orbital of an excited electron, when the probability of finding the electron near the internuclear axis is nonzero for this orbital. The short-range interaction $\hat{V}^{(s)}$ then dominates in Eq. (10).

Approximating this short-range part of the interaction by a zero-range potential, the following analytical estimator for $U^{(1)}_{n\sigma}(R)$ can be obtained [27]:

$$U^{(1)}_{n\sigma}(R) \simeq \varepsilon_{\rm nl} + 2\pi L |\psi_{nl0}(R)|^2, \tag{11}$$

which is in accordance with the Fermi result [28]. Here ε_n is the corresponding electron energy in the nl shell of the magnesium atom and the wave function $\psi_{nl0}(R)$ is the atomic wave function for the excited electron. The parameter L is the scattering length for a low-energy electron in the rare-gas-atom potential. Unfortunately it is difficult to get a similar analytical expression for the orbitals with $\lambda \neq 0$ because of zero location probability near the internuclear axis in this case. However, we can expect that the contribution of such short-range interactions should be much less for the electronic shells with $\lambda \neq 0$ and we can assume

$$U^{(1)}_{n\lambda}(R) \simeq \varepsilon_{\rm nl}, \quad \lambda \neq 0, \tag{12}$$

i.e., zero contribution in comparison with the σ orbital result. In accordance with Eq. (11) we can expect that all σ orbitals should be repulsive in such a range of internuclear separations, with the most repulsive being the $\sigma 4d$ orbital. As will be seen, this is an important point in our interpretation of the polarization spectrum in the blue wing of the Mg $3p\ ^1P_1 \rightarrow 4d\ ^1D_2$ transition perturbed by Ne or Ar.

The correction to the electron energy (11) caused by the polarization part of the effective potential (10) is very important when the internuclear separation becomes less than, but still comparable with, the distance r of the excited electron from the Mg nucleus. A corresponding contribution can be found by direct solution of the Schrödinger equation (4) only. However, we can expect here that the direct polarization interaction of the atomic ion Mg^+ with the rare-gas atom would dominate at such internuclear separations and we can select its contribution as follows:

$$U^{(1)}_{n\lambda}(R) \sim \cdots - \frac{\alpha_2}{2R^4}, \tag{13}$$

where the ellipses denote the contribution arising from the electron interaction and described by solution of Eq. (4). However, we presume that the attractive polarization contribution to the interatomic interaction will be greater for the $4d\ ^1\Pi_1$ and $4d\ ^1\Delta_2$ molecular potentials than for the $5s\ ^1\Sigma^+_0$ term because of the relatively smaller electron probability density along the internuclear axis for the $4d\ ^1\Pi_1$ and $4d\ ^1\Delta_2$ orbitals. Because of the greater overall attraction, we expect the $4d\ ^1\Pi_1$ (and possibly $4d\ ^1\Delta_2$) and $5s\ ^1\Sigma^+_0$ potentials to cross at some internuclear separation. The existence of such a crossing is important for our explanation of the observed polarization spectrum in the blue wing of the Mg $3p\ ^1P_1 \rightarrow 5s\ ^1S_0$ transition.

At yet smaller internuclear separations R (comparable to or smaller than the separations of the internal atomic electrons from their associated nuclei), direct Coulomb repulsion of atomic nuclei dominates in the interatomic interaction. In this region, the molecular potentials are mainly described by the core interaction part. All the potentials should be repulsive in this domain of internuclear separations. In principle, the potential in the highly repulsive domain can be obtained by precise *ab initio* numerical evaluation of the potential curves. Such calculations have not yet been described in the literature.

We conclude our discussion of the Mg–rare-gas interatomic interactions by showing in Fig. 1 a *qualitative* picture of potential curves for the terms correlated with atomic Mg $3s3p\ ^1P_1$, $3s5s\ ^3S_1$, $3s5s\ ^1S_0$, and $3s4d\ ^1D_2$ levels and ground-state rare-gas atoms. We expect these curves are in accordance with above general analysis and, as will be seen in the following discussion, consistent with the linear polarization data presented above. We have recently been informed via private correspondence with *E*. Czuchaj that the potentials in Fig. 1 are in qualitative agreement with his unpublished calculations.

B. Theoretical estimate of polarization signal

The measured polarization-dependent spectra are generated by photon absorption in the wings of Mg($3p\ ^1P_1 - 5s\ ^1S_0$) and Mg($3p\ ^1P_1 \rightarrow 4d\ ^1D_2$) atomic transitions in optical collisions of aligned magnesium atoms in the $3p\ ^1P_1$ state with rare-gas atoms in the ground state. The

polarization signal $P_L = P_L(\Delta)$ can be expressed in terms of a ratio of optical collision cross sections as follows

$$P_L = P_L(\Delta) = \frac{\overline{\sigma_\parallel}(\Delta) - \overline{\sigma_\perp}(\Delta)}{\overline{\sigma_\parallel}(\Delta) + \overline{\sigma_\perp}(\Delta)}, \tag{14}$$

where $\overline{\sigma_\parallel}(\Delta)$ and $\overline{\sigma_\perp}(\Delta)$ are the cross sections when the absorbed light polarization is parallel or perpendicular to the direction of the atomic alignment (z axis in major coordinate frame); Δ is the detuning from the resonance frequency of the unperturbed atomic transition. The overbar in Eq. (14) denotes the averaging over the frequency of collisions, assuming a Maxwell velocity distribution. Each cross section depends on atomic polarization assumed to be of a pure alignment type. The polarization of the atoms with angular momentum j can be defined through an alignment A [29]:

$$A = \frac{\langle 3m_z^2 - j(j+1) \rangle}{j(2j-1)}. \tag{15}$$

This definition is in accordance with the normalization condition for the quadrupole moment introduced in [30]. It can be expressed in terms of the often-used alignment parameter A_0 [31] as follows: $A = A_0(j+1)/(2j-1)$. In our case when $j=1$ the limiting values of this parameter are 1 or -2 if atoms populate Zeeman sublevels $m_z = \pm 1$ or $m_z = 0$, respectively. The polarization signal P_L depends on both frequency detuning and alignment. In the present study, the measured resonant values of P_L correspond to the limiting atomic values. The expression (14) corresponds directly to the experimentally determined polarization defined in Eq. (1).

Numerical results presented in this section are based on the semiclassical theory of optical collisions discussed first by Lewis *et al.* [32]. The theory considers a quasistatic semiclassical picture of the optical transition in a diatomic system. For definite detuning the optical transitions in the electronic subsystem are induced by the electromagnetic field when the atomic nuclei move near the vicinity of one or more Condon points located at internuclear separations R_f ($f = 1,2,\ldots$). The dependence of the transition probability on electronic and light polarization appears as a result of transformation of atomic and light density matrices into the molecular (body-fixed) frame with the assumption of classical spatial motion for colliding atoms. There have been several attempts in the literature to explain and to bring this model to a more consistent level based on a quantum treatment of atomic scattering perturbed by interaction with coherent light [18,33–35]. In these papers, the importance in a semiclassical analysis of such effects as curvature of classical trajectories and nonadiabatic dynamics of electronic subsystem has been demonstrated. All discussions have shown that the resulting semiclassical expressions for polarization-dependent cross sections are in good agreement with quantum results, both qualitatively and quantitatively.

The basic approach of the Lewis *et al.* [32] model in calculation of polarization-dependent transition probability is to ignore the interference between different classical paths for a single Condon point as well as interference coming from different Condon points. Such simplification seems normal in conditions of the present experiment, where all interference terms tend to zero because of double averaging over

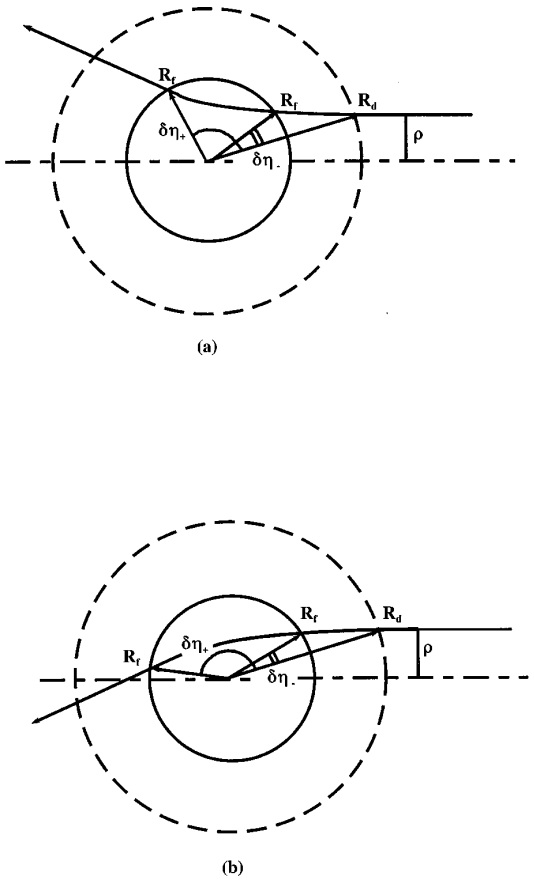

FIG. 6. Definition of geometrical terms used in theoretical modeling of the excited-state optical collision process. The deflection angle $\delta\eta_+$ is shown as a single line, while $\delta\eta_-$ is shown as a double line.

frequency of collisions and over impact parameter. The final expression of the polarization-dependent part of the optical collision cross sections $\overline{\sigma_\parallel}(\Delta)$ and $\overline{\sigma_\perp}(\Delta)$ obtained in this approximation can be explained in terms of combined transformations of light and atomic alignment components. It is of great importance for such an explanation to realize that light and atomic components are transformed in different ways. The light density matrix should be transformed into the body-fixed frame at a Condon point by simple rotation from the laboratory frame. The atomic density matrix transformation is more complicated as it represents the convolution of rotational transformation for large separations in the decoupling region [Hund's case (d), where there is negligible interatomic interaction] with a subsequent adiabatic evolution of the molecular state in a Hund's case (a) coupling scheme region (where the interaction is strong). In the final expressions for the polarization-dependent cross sections, the difference in transformation laws is indicated by the corresponding Wigner d functions depending on classical deflection angles in the $3p\ ^1\Pi_1$ and $3p\ ^1\Sigma_0^+$ potentials. It is important to note that the deflection angles depend directly on the lower term potentials, but also indirectly on the location of and size of radiative coupling at the Condon points. These deflection angles describe the rotation of the internuclear axis for nuclear motion along a classical trajectory with separation changing from the decoupling radius R_d to the Condon point location R_f. The decoupling radius R_d is an important

parameter of the model, and is estimated by the internuclear separation where the transition from Hund's case (d) to Hund's case (a) occurs. The definitions of characteristics of the model are shown in Fig. 6 for both repulsive [6(a)] and attractive [6(b)] trajectories.

Applying the general theory to analysis of the polarization-dependent absorption in the wings of the Mg($3p\ ^1P_1 \rightarrow 5s\ ^1S_0$) and Mg($3p\ ^1P_1 \rightarrow 4d\ ^1D_2$) atomic transitions, consider only dipole-allowed molecular transitions. The following excitation channels in optical collisions of magnesium and rare-gas atoms are possible: from the lower $3p\ ^1\Pi_1$ term into the upper $5s\ ^1\Sigma_0^+$, $4d\ ^1\Pi_1$, $4d\ ^1\Delta_2$, and $4d\ ^1\Sigma_0^+$ terms, and from the lower $3p\ ^1\Sigma_0^+$ state into the upper $5s\ ^1\Sigma_0^+$, $4d\ ^1\Pi_1$, and $4d\ ^1\Sigma_0^+$ terms. Corresponding expressions for the cross sections $\overline{\sigma_\parallel}(\Delta)$ and $\overline{\sigma_\perp}(\Delta)$ can be derived from the general semiclassical expressions of [18]. The procedure was described in detail in that paper and we show here the final results only.

For Condon transitions induced at an internuclear separation R_f between $3p\ ^1\Sigma_0^+$ and $5s\ ^1\Sigma_0^+$ states or between $3p\ ^1\Sigma_0^+$ and $4d\ ^1\Sigma_0^+$ states, we obtain

$$\sigma_\parallel^{(f)}(\Delta) = \frac{1}{9} 2\pi \int_0^{\rho_m^{(f)}} \rho d\rho w^{(f)}(\rho) \times \left[2 - \frac{2}{5} A[d_{00}^2(\delta\eta_-^\rho(R_f,R_d)) + d_{00}^2(\delta\eta_+^\rho(R_f,R_d))] \right], \tag{16}$$

$$\sigma_\perp^{(f)}(\Delta) = \frac{1}{9} 2\pi \int_0^{\rho_m^{(f)}} \rho d\rho w^{(f)}(\rho) \times \left[2 + \frac{1}{5} A[d_{00}^2(\delta\eta_-^\rho(R_f,R_d)) + d_{00}^2(\delta\eta_+^\rho(R_f,R_d))] \right],$$

where $w^{(f)}(\rho)$ is the reduced (independent of polarization) transition probability at the Condon point R_f, as defined below; $d_{qq}^k(\ )$ are Wigner d functions defined as in [36], which depend on deflection angle $\delta\eta_\pm^\rho(R_f,R_d)$ for atomic motion along a classical path between internuclear separations R_d and R_f and defined for incoming $(-)$ and outgoing $(+)$ parts of the trajectory with impact parameter ρ. The integrals (16) are bounded by the maximum value of impact parameter $\rho_m^{(f)}$. This value is determined by the limiting trajectory crossing (touching) the Condon point R_f. The dependence on detuning appears because of the corresponding dependence of the Condon point location, viz., $R_f = R_f(\Delta)$. The cross sections (16) depend also on the recoil energy of the collision and should be averaged over the frequency of collisions in order to be used in Eq. (14). To simplify notation we omit here and below the dependence on recoil energy.

For a transition induced at an internuclear separation R_f between $3p\ ^1\Pi_1$ and $5s\ ^1\Sigma_0^+$ states or between $3p\ ^1\Pi_1$ and $4d\ ^1\Sigma_0^+$ states, we obtain

$$\sigma_\parallel^{(f)}(\Delta) = \frac{2}{9} 2\pi \int_0^{\rho_m^{(f)}} \rho d\rho w^{(f)}(\rho) \left\{ 2 - \frac{1}{10} A[d_{00}^2(\delta\eta_-^\rho(R_f,R_d)) + 6d_{22}^2(\delta\eta_-^\rho(R_f,R_d)) + d_{00}^2(\delta\eta_+^\rho(R_f,R_d)) + 6d_{22}^2(\delta\eta_+^\rho(R_f,R_d))] \right\},$$

$$\sigma_\perp^{(f)}(\Delta) = \frac{2}{9} 2\pi \int_0^{\rho_m^{(f)}} \rho d\rho w^{(f)}(\rho) \left\{ 2 + \frac{1}{20} A[d_{00}^2(\delta\eta_-^\rho(R_f,R_d)) + 6d_{22}^2(\delta\eta_-^\rho(R_f,R_d)) + d_{00}^2(\delta\eta_+^\rho(R_f,R_d)) + 6d_{22}^2(\delta\eta_+^\rho(R_f,R_d))] \right\}. \tag{17}$$

Here, and in Eqs. (18) and (19), we have used the same notation as in Eqs. (16). For these transitions the angular momentum projection on the internuclear direction has changed by $\Delta\Lambda = \pm 1$ (perpendicular transitions) and strong interference in excitation from $^1\Pi_1$ with $\Lambda = \pm 1$ should be taken into account. This interference is described by the d_{22}^2 functions in Eqs. (17).

For transitions $3p\ ^1\Sigma_0^+ \rightarrow 4d\ ^1\Pi_1$ and $3p\ ^1\Pi_1 \rightarrow 4d\ ^1\Pi_1$, the cross sections are

$$\sigma_\parallel^{(f)}(\Delta) = \frac{2}{9} 2\pi \int_0^{\rho_m^{(f)}} \rho d\rho w^{(f)}(\rho) \left\{ 2 + \frac{1}{5} A[d_{00}^2(\delta\eta_-^\rho(R_f,R_d)) + d_{00}^2(\delta\eta_+^\rho(R_f,R_d))] \right\},$$

$$\sigma_\perp^{(f)}(\Delta) = \frac{2}{9} 2\pi \int_0^{\rho_m^{(f)}} \rho d\rho w^{(f)}(\rho) \left\{ 2 - \frac{1}{10} A[d_{00}^2(\delta\eta_-^\rho(R_f,R_d)) + d_{00}^2(\delta\eta_+^\rho(R_f,R_d))] \right\}, \tag{18}$$

In spite of the fact that the transitions have different symmetry ($3p\ ^1\Sigma_0^+ \rightarrow 4d\ ^1\Pi_1$ is perpendicular and $3p\ ^1\Pi_1 \rightarrow 4d\ ^1\Pi_1$ is parallel) they have same dependence on deflection angles.

For a Condon point associated with the $3p\ ^1\Pi_1 \rightarrow 4d\ ^1\Delta_2$ transition, we obtain

$$\sigma_{\parallel}^{(f)}(\Delta) = \frac{2}{9} 2\pi \int_0^{\rho_m^{(f)}} \rho d\rho w^{(f)}(\rho) \left\{ 2 - \frac{1}{10} A[d_{00}^2(\delta\eta_-^{\rho}(R_f, R_d)) + d_{00}^2(\delta\eta_+^{\rho}(R_f, R_d))] \right\}, \tag{19}$$

$$\sigma_{\perp}^{(f)}(\Delta) = \frac{2}{9} 2\pi \int_0^{\rho_m^{(f)}} \rho d\rho w^{(f)}(\rho) \left\{ 2 + \frac{1}{20} A[d_{00}^2(\delta\eta_-^{\rho}(R_f, R_d)) + d_{00}^2(\delta\eta_+^{\rho}(R_f, R_d))] \right\}.$$

This transition is perpendicular, but there are no interference terms from $\Lambda = \pm 1$ transitions here because the upper term has the larger angular momentum projection and such interference is thus impossible.

To evaluate the dependence of deflection angles on impact parameter in the integrals (16)–(19) we need to know the lower potentials for the $3p\ ^1\Sigma_0^+$ and $3p\ ^1\Pi_1$ states. These interaction potentials for the Mg-Ne diatomic system were evaluated by Czuchaj *et al.* [21]. The evaluated potentials were in qualitative and quantitative agreement with spectroscopic data reported by Wallace and Breckenridge [37]. For a Mg-Ar system the same potentials were evaluated by Hliwa and Daudey [22] and results were in agreement with spectroscopic data reported by Bennett *et al.* in [38] as well. However, in the case of Mg-Ar the spectroscopic study is more informative than in the case of Mg-Ne. By analysis of the spectra observed in the experiment, it is possible to recover the potential forms in the interaction region. The $3p\ ^1\Pi_1$ potential can be recovered as a Morse function by fitting vibrational components of the molecular fluorescence spectrum. The behavior of the repulsive $3p\ ^1\Sigma_0^+$ potential can be estimated by fitting the lambda-doubling constant for the observed lambda-doubling spectrum. In calculating the dependencies of deflection angles on impact parameters, we use the potentials evaluated by Czuchaj *et al.* [21] in the Mg-Ne case and empirical potentials recovered from experimental data of Bennett *et al.* [38] in the Mg-Ar case.

The asymptotic behavior of the interatomic interaction determines the limiting value of the decoupling radius (minimum possible impact parameter for the trajectory replaced in the decoupling scheme region) by the following equation:

$$\frac{\hbar}{R_d} \left(\frac{2E}{m} \right)^{1/2} \simeq \frac{\Delta C_6}{R_d^6}, \tag{20}$$

where ΔC_6 is the difference in C_6 constants for long-range interactions correlated with $\mathrm{Mg}(3p\ ^1P_1)$, E is the recoil energy, and m is the atomic reduced mass. For the Mg-Ne interaction, the corresponding value was reported by Malvern in [20] as $\Delta C_6 = 175$ a.u. We have no information about ΔC_6 for the Mg-Ar interaction and approximate it according to

$$\Delta C_6 \simeq \frac{\Delta C_6(\mathrm{Mg-rare\ gas})}{C_6^g(\mathrm{Mg-rare\ gas})} C_6^g \sim 3C_6^g, \tag{21}$$

where $C_6^g = 170$ a.u. is the ground-state constant, see [19] and ΔC_6 (Mg–rare gas) with C_6^g (Mg–rare gas) are the corresponding constants for the Mg–rare-gas system with He or Ne as the rare gas taken from Malvern [20]. Such an approximation is based on the assumption that van der Waals constants increase proportionally for excited Mg atoms in the presence of He, Ne, or Ar. It also is in accordance with the fact that the difference in the constants is mainly determined by the difference in the polarizabilities of the rare-gas atoms. For Mg-Ar this estimate leads to $\Delta C_6 = 510$ a.u. In any case, residual uncertainty in ΔC_6 is not very important for estimates of the decoupling radius R_d, for R_d depends only weakly on ΔC_6. The limiting decoupling radii estimated from Eq. (20) for the energy $E \sim 300$ K are ~ 14 a.u. for Mg-Ne and ~ 18 a.u. for Mg-Ar.

The important parameter in Eqs. (16)–(19) is the reduced transition probability $w^{(f)}(\rho)$ at the Condon point R_f:

$$w^{(f)}(\rho) = \frac{1}{\hbar^2} [V^{(f)} \tau^{(f)}(\rho)]^2. \tag{22}$$

It depends on the transition matrix element $V^{(f)}$ and on the transition time in the vicinity of the Condon point

$$\tau^{(f)}(\rho) = \left(\frac{2\pi\hbar}{\Delta F^{(f)} v^{(f)}(\rho)} \right)^{1/2}, \tag{23}$$

where $\Delta F^{(f)}$ is the difference between the slopes of the upper and lower potentials at the Condon point R_f and $v^{(f)}(\rho)$ is the radial velocity near this point. The latter depends on impact parameter ρ as follows

$$v^{(f)}(\rho) = \left[\frac{2E}{m} \left(1 - \frac{U(R_f)}{E} - \frac{\rho^2}{R_f^2} \right) \right]^{1/2}, \tag{24}$$

where the lower potential function $U(R)$ is taken at R_f.

From expressions (22)–(24) it is clear that only limited information about the upper potentials is necessary in order to calculate the cross sections in Eqs. (16)–(19), namely, the slope of the upper potentials at the Condon point R_f. In fact, substituting the partial contributions from separate Condon points into the polarization ratio (14) shows that there is no dependence on the slope difference for each partial contribution. If there are several contributions to the cross section, then there is a dependence on the slope of the difference potential. Nevertheless, it is clear that even if several Condon points make a contribution at some particular frequency to the cross section, bounds on the actual polarization ratio may still be obtained from the partial contributions estimated at each Condon point. We use these circumstances to make

theoretical estimates, using the limited available quantitative information about the upper potentials, of the possible variations in the polarization in different spectral domains. This is accomplished by the following general procedure. First, for each spectral domain we locate the possible Condon transitions that make the contributions to photon absorption. Second, for each transition we estimate the polarization ratio (14), independently taking into account possible locations of Condon points. Third, the measured value of the polarization signal is found as a mixture of these estimated values, weighted with probabilities describing the partial contribution of each Condon point. This approach ignores interference between Condon points, but still provides bounds on the polarization in the different spectral regimes.

1. Red wing of the Mg($3p\ ^1P_1 \rightarrow 5s\ ^1S_0$) transition

We expect that parallel Condon transitions between $3p\ ^1\Sigma_0^+$ and $5s\ ^1\Sigma_0^+$ molecular terms mainly determine the optical excitation in this spectral domain. A second molecular transition, $3p\ ^1\Pi_1 \rightarrow 5s\ ^1\Sigma_0^+$, which can also contribute if the potential well of the $5s\ ^1\Sigma_0^+$ term is deep enough, should lead to a smaller contribution because the corresponding Condon point should be positioned at smaller internuclear separations. For the same reason we can ignore here the possible contribution coming from the $3p\ ^1\Sigma_0^+ \rightarrow 4d\ ^1\Pi_1$ excitation channel, with subsequent Coriolis-type nonadiabatic transfer into the $5s\ ^1\Sigma_0^+$ state. The corresponding transition probability should additionally be smaller in order of magnitude because of the different signs of the slopes for the upper and lower potentials in this case, as shown in Fig. 1.

The estimates were made with cross sections (16) assuming a possible location of a Condon point in the region 11–13 a.u. for Mg-Ne and 10–14 a.u. for Mg-Ar. We suppose that uncertainties in Condon point locations are characterized by internuclear separations less than but still close to the decoupling radius for each pair. The cross sections (here and in other spectral domains) were averaged over frequency of collisions at a temperature of 330 K. Finally, we estimated polarization signal variations in the following intervals: 0.44–0.42 for Mg-Ne and 0.18–0.22 for Mg-Ar. Comparing with experimental values we can conclude that these estimates are in satisfactory agreement with experimental results. The spectral dependence can be explained by migration of the Condon point to smaller internuclear separations with increased detuning. In the case of Mg-Ne we obtain an increase of the polarization in the far red wing of the Mg($3p\ ^1P_1 \rightarrow 5s\ ^1S_0$) transition, tending to its recoil limiting value of 0.5 (see [18]), in agreement with experimental results. For Mg-Ar the experimental and theoretical data each give a smaller value than this with large detuning. A possible explanation for this is a stronger reduction in Mg-Ar of the polarization-dependent part in cross sections because of averaging over impact parameter.

2. Blue wing of the Mg($3p\ ^1P_1 \rightarrow 5s\ ^1S_0$) transition

The $5s\ ^1\Sigma_0^+$ molecular term correlates adiabatically only with the Mg($5s\ ^1S_0$) state but the other singlet terms correlate with the Mg($4d\ ^1D_2$) state. However, it is possible to produce magnesium atoms in the $5s\ ^1S_0$ state indirectly by photoexcitation of the quasimolecule into the $4d\ ^1\Pi_1$ molecular state, followed by a subsequent Coriolis-type nonadiabatic transition into the $5s\ ^1\Sigma_0^+$ state. Such an indirect excitation channel can be more effective in the blue wing of the Mg($3p\ ^1P_1 \rightarrow 5s\ ^1S_0$) atomic transition because of the larger oscillator strength [19] (approximately 30 times) for Mg($3p\ ^1P \rightarrow 4d\ ^1D$) than for Mg($3p\ ^1P \rightarrow 5s\ ^1S$). It seems reasonable that the probability of photoexcitation is higher also for the $4d\ ^1\Pi_1$ molecular state than for the $5s\ ^1\Sigma_0^+$ state. Moreover, the $4d\ ^1\Pi_1$ potential is expected to be attractive for internuclear separations inside the excitation region. Thus, for recoil collision energy close to 330 K the diatomic system should be excited into bound states in this potential. Under such conditions, all the molecules pumped into the $4d\ ^1\Pi_1$ state should pass into the $5s\ ^1\Sigma_0^+$ state because of Coriolis coupling between these terms.

An alternative channel of atomic losses via radiative transitions into the lower state is possible, but does not give a significant contribution because of the relatively much smaller probability for radiative transitions. This is readily shown by comparing the Coriolis coupling constant $V^{(c)}$ and radiative transition matrix element $V^{(f)}$. Such a comparison is done in the Appendix. For a laser pulse with 1-mJ energy and a temporal width of 6 ns, characteristic of the present experiment, the stimulated absorption or emission rate should be on the order of $10^{11}\ s^{-1}$, and the spontaneous rate around $10^8\ s^{-1}$. The Coriolis coupling should be on the order of $10^{12}\ s^{-1}$. Thus the probability of Coriolis nonadiabatic transitions from the bound $4d\ ^1\Pi_1$ state into the $5s\ ^1\Sigma_0^+$ state is expected to be much greater than radiative couplings into the lower molecular terms.

We made estimates of the polarization using cross sections described by Eqs. (18) and assuming possible excitation from both lower potentials $3p\ ^1\Pi_1$ and $3p\ ^1\Sigma_0^+$. We assumed that the Condon points should be located at internuclear separations greater than the minimum point in the attractive $3p\ ^1\Pi_1$ potential (these are approximately 9.5 a.u. for Mg-Ne [21] and 6.1 a.u. for Mg-Ar [38]) and we estimated their locations as 10–12 a.u. for Mg-Ne and 6.5–10 a.u. for Mg-Ar. The following results were obtained. For excitation via the $3p\ ^1\Pi_1 \rightarrow 4d\ ^1\Pi_1$ transition, the partial polarization signals can vary within the following intervals: -0.05 to -0.10 in the case of Mg-Ne collisions and $+0.01$ to -0.05 in the case of Mg-Ar collisions. For excitation via the $3p\ ^1\Sigma_0^+ \rightarrow 4d\ ^1\Pi_1$ transition, the possible variations are -0.31 to -0.27 in the case of Mg-Ne collisions and -0.14 to -0.08 in the case of Mg-Ar collisions. We suppose that the main contribution in the total polarization is coming from the $3p\ ^1\Pi_1 \rightarrow 4d\ ^1\Pi_1$ excitation channel because the slopes for lower and upper potentials at the corresponding Condon point have the same sign, as indicated in Fig. 1. On the contrary, the slopes of the upper and lower potentials for the $3p\ ^1\Sigma_0^+ \rightarrow 4d\ ^1\Pi_1$ Condon point have the opposite signs, which reduces the transition probability, as per Eqs. (21) and (22). Thus, we can estimate that the polarization signal for this spectral domain should be negative and less than 10% in magnitude, in agreement with experimental results.

We have to note here that the possibility of a direct adiabatic excitation via the $3p\ ^1\Pi_1 \rightarrow 5s\ ^1\Sigma_0^+$ transition was discussed earlier [18] for Mg-Ar optical collisions. It was ob-

tained there that the polarization signal should have a stable positive value close to 40% for such photoexcitation, which was in discrepancy with experimental results for large detunings. The reason for the large calculated polarization was a strong interference contribution existing in Eq. (17). In the experiment, we obtained high positive polarization only for small detuning in the blue wing. No visible interference gain and very small polarization in the far blue wing led us to a nonadiabatic explanation of the observed polarization spectrum in this spectral domain. In other words, the results of the experiment show the existence of Coriolis coupling between the $4d\ ^1\Pi_1$ and $5s\ ^1\Sigma_0^+$ potentials. We show by this example how important details of excited-term potentials can be displayed via polarization-dependent analysis of optical collisions spectra.

3. Red wing of the $Mg(3p\ ^1P_1 \rightarrow 4d\ ^1D_2)$ transition

The dynamics of photoexcitation in the wings of the $Mg(3p\ ^1P_1 \rightarrow 4d\ ^1D_2)$ transition is largely adiabatic in the upper states. The nonadiabatic coupling with the Mg–rare-gas $5s\ ^1\Sigma_0^+$ term is not important here because direct decay via the open $4d\ ^1D_2$ channels dominates in the vicinity of the $Mg(3p\ ^1P_1 \rightarrow 4d\ ^1D_2)$ resonance line.

For the red wing of the $Mg(3p\ ^1P_1 \rightarrow 4d\ ^1D_2)$ transition, excitation from the $3p\ ^1\Pi_1$ term into the $4d\ ^1\Delta_2$ and $4d\ ^1\Pi_1$ states, and from the $3p\ ^1\Sigma_0^+$ term into the $4d\ ^1\Pi_1$ state is expected. As the $3d\ ^1\Sigma_0^+$ potential is expected to be quite repulsive in the accessible range of internuclear separations, its contributions to the cross section should occur predominately to the *blue* of the resonance line. For small *red* detunings, transitions to the other terms should be induced at large internuclear separations located close to the decoupling radius. We estimate the following intervals for the Condon point locations: 11–13 a.u. for Mg-Ne and 10–14 a.u. for Mg-Ar.

Estimates of the polarization signal were made with cross sections (18) for excitations from the $3p\ ^1\Pi_1$ and $3p\ ^1\Sigma_0^+$ states into the upper $4d\ ^1\Pi_1$ state and with cross sections (19) for excitation from the $3p\ ^1\Pi_1$ term into the $4d\ ^1\Delta_2$ state. The following variations of partial polarization contributions are possible: for the $3p\ ^1\Pi_1 \rightarrow 4d\ ^1\Pi_1$ transition: -0.07 to -0.11 in Mg-Ne collisions and -0.05 to -0.11 in Mg-Ar collisions. For $3p\ ^1\Sigma_0^+ \rightarrow 4d\ ^1\Pi_1$ transitions these are -0.30 to -0.27 in Mg-Ne collisions and -0.08 to -0.12 in Mg-Ar collisions. For $3p\ ^1\Pi_1 \rightarrow 4d\ ^1\Delta_2$ photoexcitation, these are 0.04 to 0.06 for Mg-Ne collisions and 0.04 to 0.06 for Mg-Ar collisions.

The excitation from the $3p\ ^1\Pi_1$ and $3p\ ^1\Sigma_0^+$ states into the $4d\ ^1\Pi_1$ state gives *negative* contribution in the total polarization. On the contrary, the partial polarization via the $3p\ ^1\Pi_1 \rightarrow 4d\ ^1\Delta_2$ excitation channel has a positive sign. The competition between different partial channels in the formation of the total polarization signal can manifest itself in a polarization sign changing from positive to negative with detuning. The experimental polarization spectra in the red wing of the $3p\ ^1P_1 \rightarrow 4d\ ^1D_2$ atomic transition shows such a sign change in the total polarization signal for both Mg-Ne and Mg-Ar pairs. The small absolute value of polarization observed shows that the main contribution should come from excitation from $3p\ ^1\Pi_1$ into $4d\ ^1\Delta_2$ and $4d\ ^1\Pi_1$ states. Such an assumption is in agreement with the general potential behavior shown in Fig. 1, for the slopes of the upper and lower potentials have the same sign for these transitions. Note also that, because the partial contributions (as well as omitted interference contributions) have different signs, the total polarization signal tends to $\frac{1}{7}$ on resonance for the $3p\ ^1P_1 \rightarrow 4d\ ^1D_2$ atomic transition instead of 1 as it does for a $3p\ ^1P_1 \rightarrow 5s\ ^1S_1$ transition.

4. Blue wing of the $Mg(3p\ ^1P_1 \rightarrow 4d\ ^1D_2)$ transition

For the blue wing of the $Mg(3p\ ^1P_1 \rightarrow 4d\ ^1D_2)$ transition, two excitation channels are possible: $3p\ ^1\Pi_1 \rightarrow 4d\ ^1\Sigma_0^+$ and $3p\ ^1\Sigma_0^+ \rightarrow 4d\ ^1\Sigma_0^+$. Each of these gives a positive contribution for polarization and the Condon point locations are expected to be close to the decoupling radius. We take the following intervals for Condon point locations: 11–13 for Mg-Ne and 10–14 for Mg-Ar. Calculations of the polarization signal were made with cross sections described by Eq. (17) and Eq. (16) for $3p\ ^1\Pi_1 \rightarrow 4d\ ^1\Sigma_0^+$ and $3p\ ^1\Sigma_0^+ \rightarrow 4d\ ^1\Sigma_0^+$ transitions, respectively. For the partial polarization signal in the case of the $3p\ ^1\Pi_1 \rightarrow 4d\ ^1\Sigma_0^+$ transition we obtained 0.52–0.58 for Mg-Ne and 0.39–0.51 for Mg-Ar. In the case of the $3p\ ^1\Sigma_0^+ \rightarrow 4d\ ^1\Sigma_0^+$ transition we obtained 0.44–0.42 for Mg-Ne and 0.18–0.22 for Mg-Ar.

The interesting and important peculiarity in the behavior of the polarization-dependent spectrum in the blue wing of the $3p\ ^1P_1 \rightarrow 4d\ ^1D_2$ transition is the *greater* magnitude of the value of the polarization than for pure resonance photoexcitation. This fact can be clearly understood within a semiclassical description of the optical collision. As mentioned above, the resonance value of $\frac{1}{7}$ is the sum of partial contributions (and also interference terms between them) that have different signs. Some of the partial contributions are greater than the total magnitude of the polarization in this case. We have here such a situation when both Condon transitions induced in the blue wing give positive contributions and, as shown by our calculations, they are greater than 1/7. The transitions leading to the negative sign of the polarization ratio make a contribution to the spectrum in the red wing only. However, in Mg-Ne optical collisions, the experimental value of the total polarization is less than our theoretical estimates. Such a discrepancy can be probably explained by the negative influence of interference terms, which were not taken into account in our calculations. It seems reasonable that interference influence is more effective in collisions with the lighter Ne atoms. But the spectral dependence of the polarization spectra in the red and blue wings of the $3p\ ^1P_1 \rightarrow 4d\ ^1D_2$ transition is still in qualitative agreement with the asymptotic behavior of the interaction potentials shown in Fig. 1.

V. CONCLUSIONS

A combined theoretical and experimental study of excited-state optical collisions involving Mg-Ne and Mg-Ar molecules has been presented. In the study, a comprehensive experimental data set involving molecular transitions to the $5s\ ^1\Sigma_0^+$, $4d\ ^1\Delta_2$, $4d\ ^1\Pi_1$, $4d\ ^1\Sigma_0^+$, and $5s\ ^3\Sigma_1^+$ final channels from the $3p\ ^1\Pi_1$ and $3p\ ^1\Sigma_0^+$ initial electronic states were considered. A semiclassical analysis of the prob-

lem using only a qualitative picture of the interaction potentials allowed good agreement to be reached between measurements and theoretical estimates for the linear polarization spectra. Both the general size and the sign of the linear polarization degree were successfully described. The relative insensitivity to the shapes of the interatomic potentials occurs because their primary role is in determining the locations of the Condon points and the total cross section for the process. The polarization itself is determined by Wigner d functions depending on deflection angles in the lower term potentials. Because of the averaging over impact parameters, there is only a weak dependence overall on the d functions. In different spectral domains, the polarization is mainly determined by the symmetry type of the transition making the major contribution. Varying the potential form does not change the order of magnitude of the polarization signal.

The comparison of experimental and calculated results shows similar behavior for both Mg-Ne and Mg-Ar. This allows a parallel discussion of both sets of results. Moreover, such close spectral behavior indicates that the interatomic interactions are expected to be qualitatively similar for both pairs. The semiclassical analysis used in the theoretical discussion shows all important features of the spectral behavior of the linear polarization degree. However, *ab initio* numerical calculation of the highly excited Mg–rare-gas interactions seems desirable, and would be useful for more comprehensive theoretical calculations. Finally, a parallel, but completely quantum, theoretical analysis would be useful in order to provide a deeper understanding of the physics of diatomic optical excitation as well as the relationship between the semiclassical description and the fully quantum mechanical coupled channel calculations of the optical collision process.

ACKNOWLEDGMENTS

The financial support of the National Science Foundation (NSP-PHY-9504864) for this work is greatly appreciated. We also acknowledge partial support (for D.K. and S.S.) of the Civilian Research and Development Foundation (Grant RP1-263).

APPENDIX: RADIATIVE TRANSITION AND CORIOLIS COUPLING MATRIX ELEMENTS

In a semiclassical picture the probabilities of both radiative and Coriolis transitions are the square products of corresponding matrix elements and the transition times in the vicinity of Condon or crossing points. We assume that these times are the same in order of magnitude so the probabilities differ mainly by transition matrix elements. We estimate here the order of magnitude of these matrix elements.

The complex amplitude of the electric radiation field ε can be estimated from the total energy of the laser pulse ΔE_p, the pulse duration τ_p, and the spot area of the laser beam s_b as follows:

$$\varepsilon \sim \left(\frac{2\pi}{c} \frac{\Delta E_p}{s_b \tau_p} \right)^{1/2}. \tag{A1}$$

The transition matrix element of the dipole moment d_{if} connecting the initial $i = 3p\ ^1\Pi_1$ to the final $f = 4d\ ^1\Pi_1$ molecular state can be estimated by the corresponding matrix element for the resonance atomic transition. The latter can be expressed in terms of the reduced matrix element d_0. For d_{if} we obtain

$$d_{if} \sim \frac{1}{\sqrt{3}} C^{11}_{21\ 10} d_0 = -\frac{1}{\sqrt{10}} d_0, \tag{A2}$$

where we use notation of [36] for the Clebsch-Gordan coefficient. Introducing here the oscillator strength f_0 as a characteristic of the atomic dipole $3p\ ^1P_1 \rightarrow 4d\ ^1D_2$ transition [19] we can estimate the radiative transition matrix element at the Condon point R_f as follows:

$$|V^{(f)}| = |d_{if}\varepsilon| \sim \left(3 \frac{\hbar e^2}{2 m_e \omega_0} \frac{3}{10} f_0 \frac{2\pi}{c} \frac{\Delta E_p}{s_b \tau_p} \right)^{1/2}, \tag{A3}$$

where e and m_c are electronic charge and mass, respectively, and ω_0 is resonance frequency. Substituting in Eq. (A3) the values $\Delta E_p \sim 1$ mJ, $\tau_p \sim 6$ ns, $s_b \sim 0.1$ cm^2, wavelength $\lambda_0 \approx 553$ nm, and oscillator strength $f_0 \sim 0.15$, we obtain $|V^{(f)}|/\hbar \sim 1.3 \times 10^{11}$ s^{-1}. Thus the excitation rate greatly exceeds the typical spontaneous $E1$ rate of $\sim 10^8$ s^{-1}.

The Coriolis coupling constant for a Landau-Zener type of nonadiabatic transition located at the crossing point R_c can be expressed as follows:

$$V^{(c)} \cong \hbar v_\infty \frac{\rho}{R_c^2} \overline{j_\perp}, \tag{A4}$$

where v_∞ is the recoil velocity for infinitely separated colliding atoms, $\overline{j_\perp} \sim O(1)$ is the matrix element of electronic angular momentum between the $4d\ ^1\Pi_1$ and $5s\ ^1\Sigma_0^+$ states, which is of order unity for allowed Coriolis-induced transitions. We estimate the internuclear separation R_c and impact parameter ρ in order of magnitudes as $R_c \sim \rho \sim 10$ a.u. The recoil velocities for typical energy $E \sim T \sim 300$ K are 6.7×10^4 cm/s (Mg-Ne) and 5.7×10^4 cm/s (Mg-Ar). Substituting these values into Eq. (A4) we obtain the following estimates for Coriolis coupling constants 1.3×10^{12} s^{-1} and 1.1×10^{12} s^{-1} for Mg-Ne and Mg-Ar collisions, respectively.

[1] *Atomic and Molecular Beams Methods 1*, edited by Giacinto Scoles (Oxford University Press, New York, 1988).
[2] A. H. Zewail, Science **242**, 1645 (1988); L. R. Kundekar and A. H. Zewail, Annu. Rev. Phys. Chem. **41**, 15 (1990).
[3] K. Burnett, Phys. Rep. **118**, 339 (1985).
[4] P. D. Kleiber, W. C. Stwalley, and K. M. Sando, Annu. Rev. Phys. Chem. **44**, 13 (1993).
[5] W. H. Breckenridge, C. Jouvet, and B. Soep, in *Advances in Metal and Semiconductor Clusters*, edited by M. Duncan (JAI Press, Greenwich, 1995), Vol. 3.
[6] P. R. Brooks, Chem. Rev. **88**, 407 (1988).
[7] D. M. Neumark, Annu. Rev. Phys. Chem. **43**, 153 (1992).
[8] E. Hirota, *High-Resolution Spectroscopy of Transient Molecules* (Springer-Verlag, New York, 1985).
[9] P. Arrowsmith, S. H. P. Bly, P. E. Charters, P. Chevrier, and J. C. Polanyi, J. Phys. Chem. **93**, 4716 (1989).
[10] D. A. Olsgaard, M. D. Havey, A. Sieradzan, and R. Lasell, Phys. Rev. Lett. **69**, 745 (1992).
[11] R. A. Lasell, D. A. Olsgaard, M. D. Havey, and D. V. Kupriyanov, Phys. Rev. A **50**, 423 (1994).
[12] I. V. Hertel, H. Schmidt, A. Baering, and E. Meyer, Rep. Prog. Phys. **48**, 3785 (1985).
[13] J. P. J. Driessen, C. J. Smith, and S. R. Leone, Phys. Rev. A **44**, 1431 (1991).
[14] C. J. Smith, E. M. Spain, M. J. Dalberth, and S. R. Leone, J. Chem. Soc. Faraday Trans. **89**, 1401 (1993).
[15] J. P. J. Driessen and S. R. Leone, J. Phys. Chem. **96**, 6136 (1992).
[16] J. Grosser, D. Gundelfinger, A. Maetzing, and W. Behmenburg, J. Phys. B **27**, L367 (1994); J. Grosser, D. Hohmeier, and S. Klose, *ibid.* **29**, 299 (1996).
[17] D. A. Olsgaard, R. A. Lasell, M. D. Havey, and A. Sieradzan, Phys. Rev. A **48**, 1987 (1993).
[18] D. V. Kupriyanov, Chem. Phys. **193**, 141 (1995).
[19] A. A. Radzig and B. M. Smirnov, *Reference Data on Atoms, Molecules, and Ions* (Springer-Verlag, Berlin, 1985).
[20] A. R. Malvern, J. Phys. B **11**, 831 (1978).
[21] E. Czuchaj, H. Stoll, and H. Preuss, J. Phys. B **20**, 1487 (1987).
[22] M. Hliwa and J. P. Doudey, Chem. Phys. Lett. **153**, 471 (1988).
[23] E. Czuchaj, F. Rebentrost, H. Stoll, and H. Preuss, Chem. Phys. Lett. **182**, 191 (1991).
[24] L. K. Kahn, P. Baybutt, and D. G. Truhlar, J. Chem. Phys. **65**, 3826 (1976).
[25] E. E. Nikitin and S. Ya. Umanskii, *Theory of Slow Atomic Collisions* (Springer, Berlin, 1984).
[26] G. K. Ivanov, Opt. Spectrosk. **37**, 636 (1974); **39**, 384 (1975) [Opt. Spectrosc. **37**, 361 (1974); **39**, 474 (1975)].
[27] M. Ya. Ovchinnikova, Zh. Eksp. Teor. Fiz. **49**, 275 (1965) [Sov. Phys. JETP **22**, 194 (1996)].
[28] E. Fermi, Nuovo Cimento **11**, 157 (1934).
[29] D. V. Kupriyanov and O. S. Vasyutinskii, Chem. Phys. **171**, 25 (1993).
[30] L. D. Landau and E. M. Lifshitz, *Quantum Mechanics* (Pergamon Press, Oxford, 1965).
[31] U. Fano and J. H. Macek, Rev. Mod. Phys. **45**, 553 (1973).
[32] E. L. Lewis, M. Harris, W. J. Alford, J. Cooper, and K. Burnett, J. Phys. B **16**, 553 (1983).
[33] F. Rebentrost, R. Best, and W. Behmenburg, J. Phys. B **20**, 2627 (1987).
[34] R. J. Bieniek, Phys. Rev. A **35**, 3663 (1987).
[35] R. J. Bieniek, P. S. Julienne, and F. Rebentrost, J. Phys. B **24**, 5103 (1991).
[36] D. A. Varshalovich, A. N. Moskalev, and V. K. Khersonskii, *Quantum Theory of Angular Momentum* (World Scientific, Singapore, 1988).
[37] I. Wallace and W. H. Breckenridge, J. Chem. Phys. **98**, 2768 (1993).
[38] R. R. Bennett, J. C. McCafrey, I. Wallace, D. J. Funk, A. Kowalski, and W. H. Breckenridge, J. Chem. Phys. **90**, 2139 (1989).